JAIST Repository
https://dspace.jaist.ac.jp/

Title	グラフェンナノリボン-バンド間トンネルトランジスタにおける物理特性の研究
Author(s)	Hammam, Ahmed Mohammed Mohammed
Citation	
Issue Date	2017-09
Type	Thesis or Dissertation
Text version	ETD
URL	http://hdl.handle.net/10119/14838
Rights	
Description	Supervisor:水田　博，マテリアルサイエンス研究科，博士

JAIST
JAPAN
ADVANCED INSTITUTE OF
SCIENCE AND TECHNOLOGY

Japan Advanced Institute of Science and Technology

ABSTRACT
Study of the Physical Properties of Graphene Nano-Ribbon Band-to-Band Tunnel Transistors

Laboratory: Mizuta Lab
Student No.: S1340207
Name: Ahmed Mohammed Mohammed Hammam

1 Background

The performance of Very Large Scale Integration circuits has been gradually improved by scaling down device dimensions. However, the heat dissipation issue is becoming more critical and harder to solve for CMOS while keeping the previous scaling down trend. Thus, due to the subthreshold swing (SS) of the Metal-oxide-semiconductor field effect transistor (MOSFET) is limited to 60 mV/decade, it is hard to scale the drain voltage V_D while increasing the speed and maintaining low off-state power dissipation. Tunnel Field Effect Transistors (TFET) have attracted much interest due to their low OFF current (I_{OFF}) and the possibility of reaching a SS below the limit (60 mV/decade) of standard CMOS technology. However, all experimentally realized TFETs based on conventional semiconductors exhibit low ON-state current (I_{ON}), which limits their usefulness in integrated circuits.

Due to the atomically thin nature, width tunable bandgap, and low effective mass, Graphene Nano-Ribbons (GNR) is seen as one of the most promising materials to overcome the limitations of conventional TFETs. However, realizing a reliable GNR-TFET is quite challenging. To introduce a reasonable energy gap to the GNR, the width should be around 10 nm, which is a very tough task to achieve. Also, GNR edge states and quantum condiments come to the pictures at such narrow ribbons. All of these challenging and difficulties should be taken into consideration during the fabrication of the GNR-TFET

2 Aim

There has not been any experimental report of GNR-TFET operation until now. Therefore, this dissertation investigates and studies the feasibility of realizing GNR-TFETs and aim to:

- Demonstration of band-to-band tunneling(BTBT) based GNR-TFET
- Demonstrate I_{ON} > conventional TFET

This includes understanding the physics of the GNR *p-n* junction because a TFET is, in principle, a reverse biased *p-i-n* junction. To achieve my target, first I planned to fabricate and study physical properties of GNR *p-n* junction, secondly fabricate and study GNR-TFET.

3 Experimental Results and discussion

GNR *p-n* Junction

3.1.1 Realization of GNR *p-n* junction

In the current work, our GNR width is ~ 15-nm with an estimated E_g in the order of 44 meV. The GNR used here has been fabricated from single layer CVD graphene supported by a SiO_2/Si substrate. Two independent top gates, with separation of ~ 40 nm, are used to define the GNR *p-n* junction under investigation (see Fig. 1a). To confirm the functionality of each gate and the performance of the GNR, the I_d measured as a function of gate voltage (V_{Tg}) at constant V_d. Room temperature measurement (shown in Fig. 1b), in general, demonstrates that all the gates including back-gate show good I_d modulation. To achieve all the possible coping combinations of the device, one of the top gate voltages (V_{Tg1} and V_{Tg2}) is swept from - 4V to 4V (-5V to 5V at low temperature) with the other top gate voltage stepped in the same range. V_d is fixed at 3 mV for all measurements at 25 K and above, and 12 mV below due to the high current suppression at lower

temperatures. The contour plot of I_d as a function of both top gate voltages illustrates the key features of our device (see Fig. 1c). First, four distinct regions belonging to the four possible configurations (*pn, np, pp, and nn*) are clearly visible. Secondly, the low current region is slightly slanted, which means that there is a weak capacitive interaction between the two top gates. Therefore, GNR *p-n* junction successfully realized.

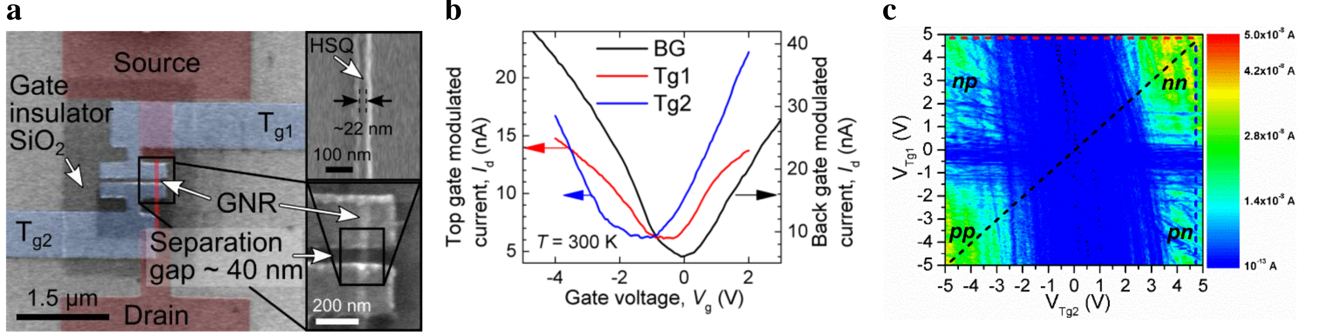

Figure 1. (a)SEM image of the two top gate device structures. Fake colours are applied for better understanding. (b) Back gate (bg) modulation and Top gate modulation. (c) Contour plot of drain current as function of the top gate voltages at T = 10 K. Drain voltage Vd is 12 mV. The clearly defined doping regions induced by the electrostatically doping are indicated by np, nn, pn, and pp, respectively.

3.1.2 Transport characteristics of GNR *p-n* junction

The drain current (I_d) at 10 K is shown for different gating configurations in Fig. 2. When using the global back gate (Fig. 2a), a symmetric modulation is observed with some random oscillation around the CNP at V_g = -0.5 V with ON/OFF ratio ~ 10^5. The symmetric modulation is consistent with the 300 K measurement shown in Fig. 1b. In contrast to the global back gate (Fig. 2a), when fixing one of the top gates and sweeping the other one, a remarkable step change in the drain current is observed. For fixed V_{Tg1} = 4.9 V (Fig. 2b, corresponding to np biasing), the step change with a rate of ~ 42 mV/dec over a range five order of magnitude in drain current (~$5x10^5$) is observed at $V_{Tg2} \approx$ -1 V. The OFF-state current is at least one order of magnitude lower than for the back gate modulated current. In case of a fixed V_{Tg2} = 4.9 V (Fig. 2c, *pn* biasing), the rate of the step change at $V_{Tg1} \approx$ -0.8 V is ~32 mV/dec but only over a range of four order of magnitude in drain current (~$1.1x10^4$). Furthermore, the current is only very slightly affected by the V_{Tg1} outside of the suppression region.

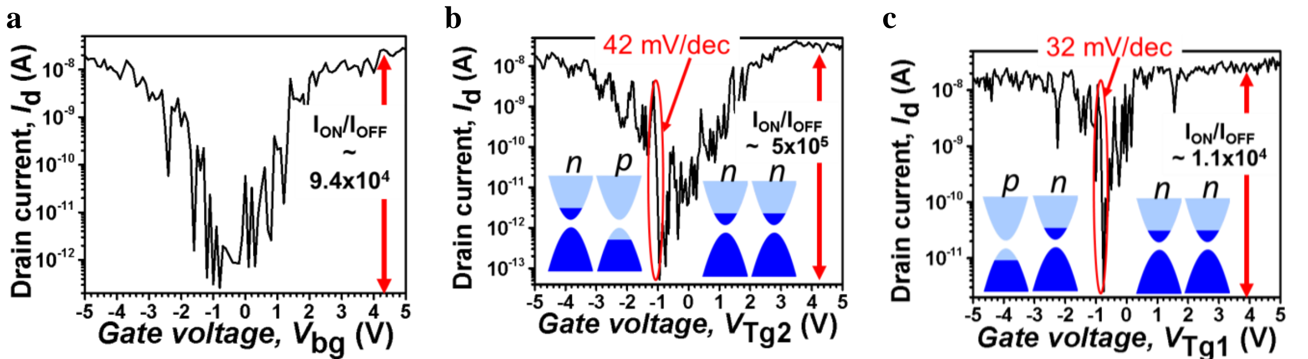

Figure. 2 Drain current as a function of gate voltage at T = 10K and V_d = 10 mV: (a) Back gate voltage sweep (b) T_{g2} sweep at V_{Tg1} = 4.9 V. The device is switched from nn configuration to pn configuration by sweeping V_{Tg2} from 5 V to -5 V (forward biasing (c) V_{Tg1} sweep at V_{Tg2} = 4.9 V (reverse biasing) showing similar characteristics with 32 mV/decade in the sharp switching region over four orders of magnitude

3.1.3 Origin of sharp switching

The sharp switching was observed in the np and pn biasing condition at low temperature (Fig. 2b and c), when one of the gates is biased so that the valence band edge in the variable gate region is lifted into the bias window and at the same time above the conduction band edge in the fixed gate region. We can thus sketch the simplified band structure of the p-n junction as shown in Fig. 3. In the uniformly nn-doped state, a large drift current is enabled. As the energy of the band edges in the T_{g2} region are shifted up, the drift current is reduced and a thermally activated leakage current dominates the transport. Finally, as the band overlap occurs, the tunneling width W_T is abruptly reduced. As the tunneling window is formed in the bias window (between E_{FD} and E_{FS}), the large number of available charge carriers enables the increase of the drain current over five orders of magnitude with the sharp slope. As the tunneling energy window is further increased (V_{Tg2} is further decreased), the sharp switching saturates because the transport through the remaining parts of the channel limit the allowed current.

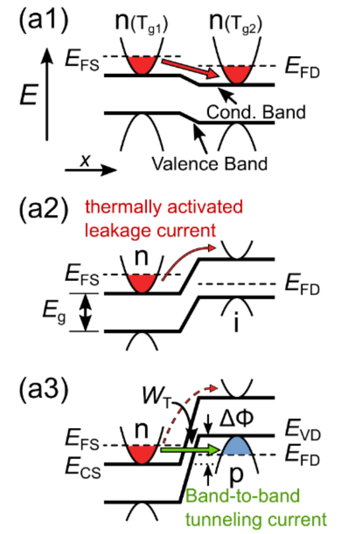

Figure 3. Proposed band structure model of p-n junction.

Triple-Gate GNR-TFET

BTBT behavior was reported in the GNR *p-n* junction with two top gates. However, to make the device usable as a switch with superior behavior to the silicon MOSFET, it is necessary to control the intrinsic region. This can be achieved by fabricating a third top gate. Here we report, for the first time, band-to-band tunneling in a sub-10 nm GNR controlled triple top gate transistor. AFM image of the fabricated device is shown in Fig. 4a. the narrower GNR at the center of the channel and wider graphene acting as extension of the source and drain contacts are covered by the SiO_2 and top gates but still visible. Detailed dimensions of the device are presented in Table 1.

Table 1. Tri-gate device dimensions

L_{ch}	L_{Tg1}	L_{Tg2}	L_{Tg2}	d
500 nm	280 nm	70 nm	280 nm	30 nm

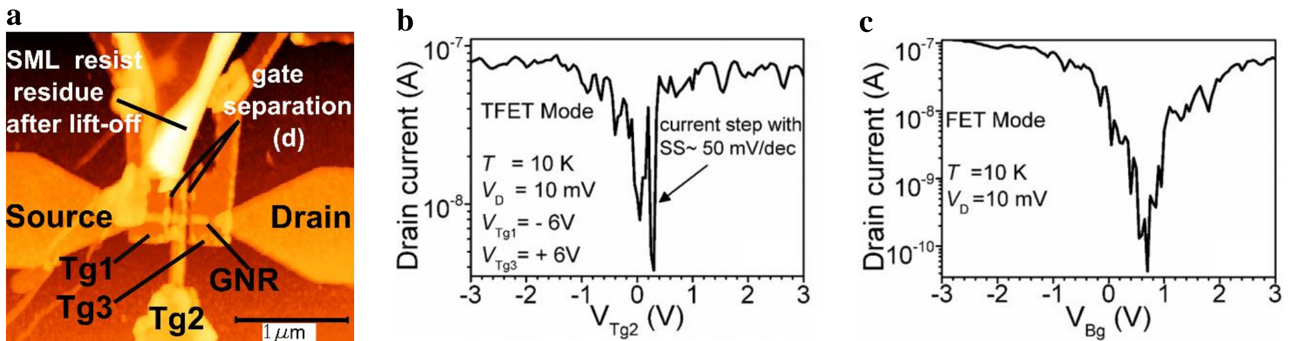

Figure 4 (a) AFM image of the measured device shows the separation d ~ 30 nm between the top gates above the GNR, and the HSQ etching mask of ~ 30 nm width. (a) Drain current as a function of the back-gate voltage (FET mode). Top gates are floating. (b) TFET mode: The middle gate voltage (V_{Tg2}) is swept from -3 V to 3 V, while the V_{Tg1} and V_{Tg3} are fixed at -6 V and 6 V, respectively.

3.2.1 Transport characteristics

To ensure that the carrier transport characteristics through our device is due to the BTBT, we compare the characteristics of the device in the TFET (realized by top gates) (shown in Fig. 4b) and FET (realized by back gate) configurations (shown in Fig. 4c), respectively. In all measurements shown here the source-drain voltage (V_D) is fixed at 10 mV ($V_D < E_g/2$) to decrease the ambipolarity and I_{OFF}. As can be seen in Fig. 4c, in the case of FET mode, the drain current (I_D) shows clear ambipolar behavior with high I_{ON}/I_{OFF} ratio of ~ 2.5×10^3. In contrast, in the TFET mode I_D shows a

steep current jump followed by a remarkable current saturation (I_{ON}) when V_{Tg2} is swept in the positive direction (*n*-type conduction), see Fig. 4b. However, the clearly different transfer characteristics between the two modes indicate that the carrier's injection mechanisms are different. Therefore, to clarify the difference between the two modes, I will discuss the temperature dependence of the SS next.

3.2.2 Temperature dependence of subthreshold slope

The I_D -V_{Tg2} characteristics of our device operated in TFET mode between 10 and 300 K are shown in Fig. 5a. At low temperature, the current has a sharp slope (SS ~ 47 mV/dec). By increasing the temperature, the current transition slope decreases (larger SS). The extracted values of SS from the I_D-V_{Tg2} curves in Fig. 5b show temperature independence up to 40 K, followed by a gradual increase with temperature up until 100 K (SS ~ 180 mV/dec). Above 100 K, an exponential increase of SS is observed, finally reaching 8.4 V/dec at 300 K. On the other hand, in the FET mode, the SS shows linear temperature dependence over the whole range of temperatures (10 to 300 K), similar to the thermal limit of the MOSFET (see Fig. 5c). This remarkable inversion of the SS, together with the temperature independence at low temperature in the TFET configuration is a substantial evidence that the drain current does not originate from the thermionic emission and is due to BTBT.

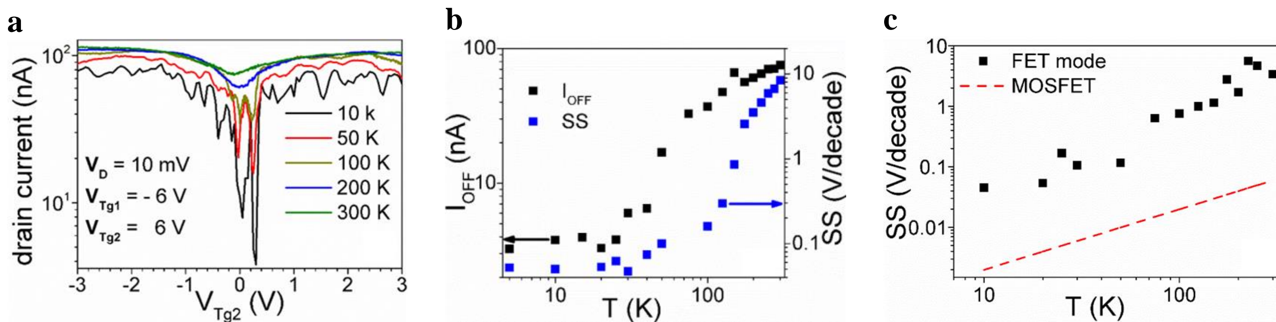

Figure 5. (a) I_D-V_{Tg2} at different temperatures for TFET mode. V_{Tg1} and V_{Tg3} are fixed at – 6 V and + 6 V, respectively, and V_D is 10mV. (b) The extracted values of I_{OFF} and SS from I_D-V_{Tg2} curves in (a). (c) SS as a function of temperature of our device in FET mode and the thermal limit of the MOSFET

THESIS TABLE OF CONTENTS

		Page No.
Chapter 1	INTRODUCTION	1
Chapter 2	GRAPHENE NANO-RIBBON BAND-TO-BAND TUNNEL MODEL	9
Chapter 3	FABRICATION AND EXPERIMENTAL SETUP	21
Chapter 4	SHARP SWITCHING BEHAVIOUR IN GNR P-N JUNCTION	36
Chapter 5	GNR TUNNEL FIELD EFFECT TRANSISTOR	52
Chapter 6	SUMMARY AND FUTURE WORK	59
REFERENCES		65
List of Publications		74

Keywords: Graphene nano-ribbon, Band-to band tunneling, Field effect transistor

List of Publications

1- **Ahmed M. M. Hammam**, M.E. Schmidt, M. Muruganathan, H. Mizuta, **Sharp switching behaviour in graphene nanoribbon p-n junction**, Carbon. 121 (2017) 399–407. doi:10.1016/j.carbon.2017.05.097.

2- **Ahmed M. M. Hammam**, M.E. Schmidt, M. Muruganathan, Shunei Suzuki, H. Mizuta, **Sub-10 nm graphene nano-ribbon tunnel field-effect transistor**, accepted